



Design of free patterns of nanocrystals with ad hoc features via templated dewetting

M. Aouassa, I. Berbezier, L. Favre, A. Ronda, M. Bollani, R. Sordan, A. Delobbe, and P. Sudraud

Citation: [Applied Physics Letters](#) **101**, 013117 (2012); doi: 10.1063/1.4730620

View online: <http://dx.doi.org/10.1063/1.4730620>

View Table of Contents: <http://scitation.aip.org/content/aip/journal/apl/101/1?ver=pdfcov>

Published by the [AIP Publishing](#)

Articles you may be interested in

[Ordered arrays of Si and Ge nanocrystals via dewetting of pre-patterned thin films](#)

J. Appl. Phys. **113**, 064908 (2013); 10.1063/1.4790713

[One-dimensional lateral growth of epitaxial islands on focused ion beam patterned substrates](#)

J. Appl. Phys. **113**, 044308 (2013); 10.1063/1.4778708

[Process considerations for layer-by-layer 3D patterning of silicon, using ion implantation, silicon deposition, and selective silicon etching](#)

J. Vac. Sci. Technol. B **30**, 06FF05 (2012); 10.1116/1.4756947

[Control of semiconductor quantum dot nanostructures: Variants of Si x Ge 1 - x / Si quantum dot molecules](#)

J. Vac. Sci. Technol. B **29**, 011029 (2011); 10.1116/1.3533938

[Site-controlled growth of Ge nanostructures on Si\(100\) via pulsed laser deposition nanostenciling](#)

Appl. Phys. Lett. **91**, 113112 (2007); 10.1063/1.2783473



AIP | Journal of
Applied Physics

Journal of Applied Physics is pleased to
announce **André Anders** as its new Editor-in-Chief

Design of free patterns of nanocrystals with ad hoc features via templated dewetting

M. Aouassa,¹ I. Berbezier,^{1,a)} L. Favre,¹ A. Ronda,¹ M. Bollani,² R. Sordan,² A. Delobbe,³ and P. Sudraud³

¹IM2NP, CNRS, AMU, Marseille, France

²LNES, Como, Italy

³Orsay Physics, Fuveau, France

(Received 20 March 2012; accepted 30 May 2012; published online 5 July 2012)

Design of monodisperse ultra-small nanocrystals (NCs) into large scale patterns with ad hoc features is demonstrated. The process makes use of solid state dewetting of a thin film templated through alloy liquid metal ion source focused ion beam (LMIS-FIB) nanopatterning. The solid state dewetting initiated at the edges of the patterns controllably creates the ordering of NCs with ad hoc placement and periodicity. The NC size is tuned by varying the nominal thickness of the film while their position results from the association of film retraction from the edges of the lay out and Rayleigh-like instability. The use of ultra-high resolution LMIS-FIB enables to produce monocrystalline NCs with size, periodicity, and placement tunable as well. It provides routes for the free design of nanostructures for generic applications in nanoelectronics. © 2012 American Institute of Physics. [<http://dx.doi.org/10.1063/1.4730620>]

During the last decades, mobile electronic products have invaded our daily lives by increasing their innovation, technical achievement, and marketability. Many of these devices require flash memories where a floating-gate structure forms the primary technology. In such a situation, conventional nonvolatile memory suffers from certain physical limitations. In order to overcome these limitations, it has been proposed to use nanocrystals (NCs) as charge storage elements embedded in the gate oxide of a field-effect transistor.^{1–6} Various processes have been developed to elaborate silicon (Si) or germanium (Ge) NCs, including self-assembly,^{7–9} precipitation,¹⁰ ion implantation,^{11–14} and annealing.^{15–17}

Si and Ge NCs for which the local physical properties govern their electronic response have recently been fabricated.^{18–21} The synthesis make use of dewetting which involves the transformation of a bi-dimensional (2D) thin film into an array of isolated three-dimensional (3D) islands due to a morphological instability.²² It is the balance between the surface and interfacial energies of the thin film and substrate that defines the 3D islands morphology.^{23–27} The energetic informs about the global energy of the system, but the evolution of each component depends on the local energetic changes in its immediate vicinity.^{28–30}

It was reported that when a thin film is unstable, it first develops a series of holes at the film/substrate interface (homogeneous dewetting), then the holes evolve and grow laterally while islands form on the edges of the dewetted front, and finally, the dewetted areas come into contact to form a fully dewetted layer.^{31–33} In the case of crystalline thin films, the holes nucleation was described by a breaking time which follows an exponential evolution with temperature.³⁴ The second regime (retraction) is controlled by the surface diffusion from the edges of the holes. The third regime (coalescence) requires to overcome an additional nucleation barrier to come into contact.³⁵ The islands represent a metastable

morphological state and could undergo coarsening on a time-scale commonly longer than the experiment.^{36,37} In the case of amorphous Ge layer (a-Ge) on a silicon dioxide (SiO₂)/Si substrate, ultra-small and dense Ge hemispheric NCs with high aspect ratio can be produced.^{38,39} In these conditions, the shape transformation results from two energy driven phenomena implying first the crystallization of the amorphous layer and second the redistribution of the matter around the crystalline clusters.⁴⁰

In all the situations, after dewetting, the surface is fully covered by NCs with broad size distribution that are randomly distributed over the surface. These NCs have been demonstrated to exhibit remarkable properties such as single-electron tunnelling, ballistic transport, and light emission.^{41–45} However, their size dispersion and random spatial distribution produce fluctuations from device to device and charge leakage.⁴⁶

The aim of this study is to design specific patterns of semiconductor NCs fully adapted to memory applications. Here, we report a design concept, based on the dewetting of pre-patterned thin films (amorphous and single crystal). In this process (heterogeneous dewetting), the solid state dewetting initiated at the edges of the layout controllably creates free patterns of NCs with ad hoc placement and length scales different from the original patterns.⁴⁷ The NCs size is tuned by varying the nominal thickness of the film while their position results from the association of processes such as the film retraction initiated at the edges of the patterns and the break-up of the film perpendicular to the dewetting edges due to a Rayleigh-like instability.

The samples investigated are (i) ultra-thin crystalline silicon on insulator (SOI) layers (ref. c-Si); (ii) amorphous germanium and silicon layers deposited on SiO₂ thermal oxide/Si substrate (ref. a-Ge and a-Si, respectively), and (iii) patterned ultra-thin crystalline SOI (ref. p-Si).⁴⁸ They are single-crystal Si(001) films, with thickness between 5 and 20 nm, bonded to a 150 nm thick SiO₂ layer on a standard

^{a)}E-mail: isabelle.berbezier@im2np.fr.

Si(001) wafer. The thickness of the top layer was varied using chemical etching cycles. The thickness homogeneity and the crystalline quality of the c-Si after etching were determined by high resolution transmission electron microscopy (HRTEM). The a-Ge and a-Si layers, with thickness between 0.5 and 5 nm, were deposited on a SiO₂ thermal layer, using a RIBER solid source molecular beam epitaxy (SSMBE) system with a background pressure $\sim 10^{-11}$ Torr.

Patterns consisting of lattices of lines and holes were prepared by electron beam lithography (EBL) or by liquid-metal ion source focused ion beam (LMIS-FIB) nanowriting.⁴⁹ EBL patterns were created on Si/SiO₂ or Ge/SiO₂ systems cleaned by an ultrasonic treatment with organic solvents. Then a polymethylmethacrylate (PMMA) layer was deposited by spinning (4000 rpm) and baked for 1 h at 160 °C after resist deposition. Scanning electron microscopy (SEM) was performed using a Philips XL30 SFEG SEM with a Raith Elphy Quantum lithography attachment and a Scanservice beam blanker. By reactive ion etching (RIE), about 11 nm of SOI were etched (using 50 sccm of CF₄ at a power of 50 W and a pressure of 6 mTorr). For every exposure, the patterned area was $25 \times 25 \mu\text{m}^2$ with lines regularly spaced between 100 nm and 1 μm . Figure 1 gives the typical morphology of EBL patterns on Si/SiO₂/Si substrate (lines along [100] and [110]). A single sample presents six geometries, the first three with lines along [110] direction and the others with lines along [100].

Large $100 \times 100 \mu\text{m}^2$ patterns with complex geometries, such as arrays of linear, square, and circular features, were also created by focused ion beam (FIB) nanomilling carried out in a Tescan LYRA1 XMH dual-beam FIB workstation operating at 30 keV. This FIB is equipped with a mass-filtered ultra-high resolution focused ion beam COBRA-type FIB from Orsay Physics, which has an ultimate resolution of 5 nm (using Ga⁺ ions). Patterning was performed using either single element (Ga⁺ ions) or AuGe alloy sources (Au⁺⁺ or Ge⁺ ions).^{50,51} The metallic incident ions implanted in the substrate at the end of the patterning process are removed by successive cleaning cycles involving both chemical cleaning (HCl solution) and thermal cleaning. After patterning, all samples were analyzed by SEM and atomic force microscopy (AFM) in air to check the depth and quality of patterns.

After *ex situ* chemical cleaning, the samples are immediately transferred under clean room atmosphere to the MBE chamber where they are *in situ* cleaned at low temperature (600 °C for 30 min) to remove the contaminants at the Si surface. Dewetting is obtained by *in situ* ultra-high vacuum (UHV) annealing at temperatures 650-800 °C.

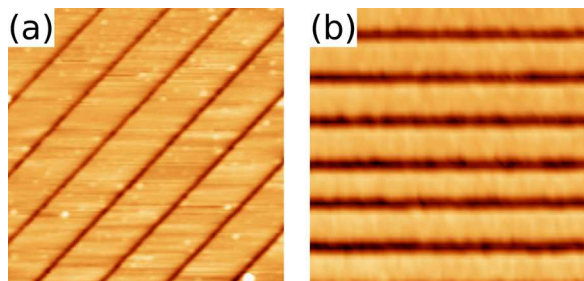


FIG. 1. Typical EBL arrays of lines along (a) [100] and (b) [110] with a periodicity of 500 nm (scan areas are $3 \times 3 \mu\text{m}^2$).

We first measured the morphological evolution of the NCs produced by homogeneous dewetting for the three systems: c-Si, a-Si, and a-Ge on top of SiO₂/Si substrate. The results show that the temperature and time of annealing (between 650 and 800 °C and 25–120 min, respectively) do not affect the NC diameter (Φ). The latter depends only on the nominal thickness (h) of the thin film, following a linear evolution $\Phi \sim k \cdot h$ with $k_{\text{Si}} = 20$ and $k_{\text{Ge}} = 7$ for Si and Ge, respectively, when annealed for instance at 750 °C for 120 min (Fig. 2(a)). These evolutions are related to the energetic balance of the system (surface and interfacial energies) since NCs represent the pseudo-equilibrium shape of the Si/SiO₂ or Ge/SiO₂ systems; independently of the dynamics to reach the equilibrium. It depends on the chemical species of the dewetted layer. The balance and contact angle differ significantly for Si and Ge as testified by the very different aspect ratios of the NCs $A = H/\Phi$ (where H is the NCs height) since $A_{\text{Si}} = 0.3$ and $A_{\text{Ge}} = 0.8$ for Si and Ge, respectively. This explains why the NC size evolution is the same for a-Si and c-Si although the dynamics of dewetting are very different.³⁵ Continuous thin films (amorphous and crystalline) on flat surfaces dewet to form NCs with broad distributions of sizes and spacings.⁴⁷

However, it has recently been shown that dewetting of pre-patterned films with regular pit-like topographic features can lead to ordered arrays of near mono-disperse NCs.^{52,53}

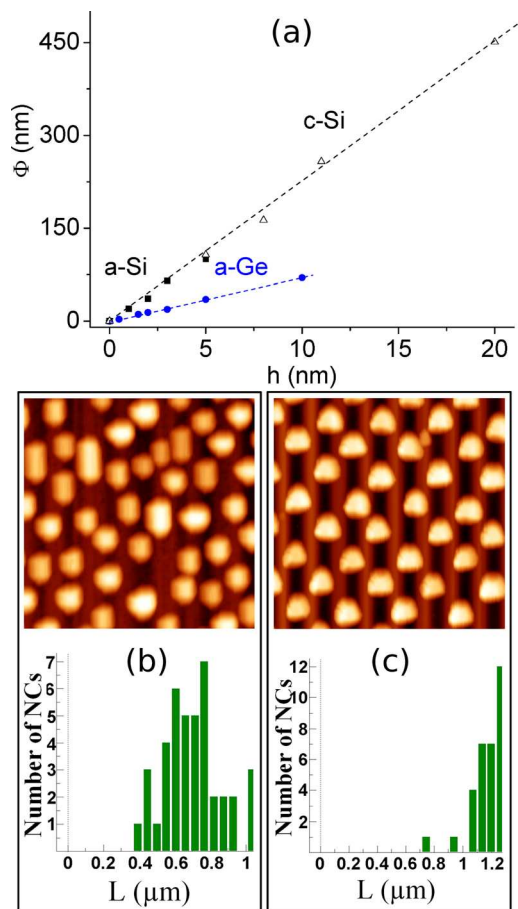


FIG. 2. (a) Size evolution of Si and Ge NCs as a function of the nominal thickness of the dewetted film for (∇) c-Si, (\blacksquare) a-Si, and (\bullet) a-Ge. AFM images and perimeter L (μm) histograms of Si NCs formed after 120 min annealing at 750 °C by (b) homogeneous dewetting and (c) heterogeneous dewetting (scan areas are $3 \times 3 \mu\text{m}^2$).

In these conditions, the so-called heterogeneous dewetting occurs. For comparison, the size of the NCs obtained by homogeneous (Fig. 2(b)) and heterogeneous (Fig. 2(c)) dewetting are presented. The images and histograms evidence the better size homogeneity in the case of heterogeneous dewetting. We first note that the size (density) of NCs is systematically larger on the patterned areas than on the continuous film. This is attributed to the confinement of matter coming from the two opposite dewetted sides of the mesas, which favors the coalescence of NCs.

Fig. 3 shows the heterogeneous dewetting initiated by EBL lines patterned along [001] or [110]. The different steps of heterogeneous dewetting observed are (i) the periodic breaking of the film perpendicular to the dewetting front following a Rayleigh-like instability (Fig. 3(a)); (ii) the regular nucleation of NCs along these cracks from which the matter is retracting (Fig. 3(b)). For patterns with periodicity $\leq 1 \mu\text{m}$, the NCs systematically form in the middle of the mesa. (iii) The proper alignment of NCs parallel to the dewetting front into periodic arrays. A perfect bi-dimensional design with one NC per period is obtained when the size of the NCs matches the period of the patterns (Fig. 3(c)). The same evolution is observed with EBL lines along [100], but the NCs undergo a shape transformation. In a first step, the NCs sides follow the dewetted fronts (along the [100] EBL lines) and exhibit (100) facets (Figs. 3(d) and 3(e)), while in a second step, they rotate by 45° to reach the equilibrium shape of sili-

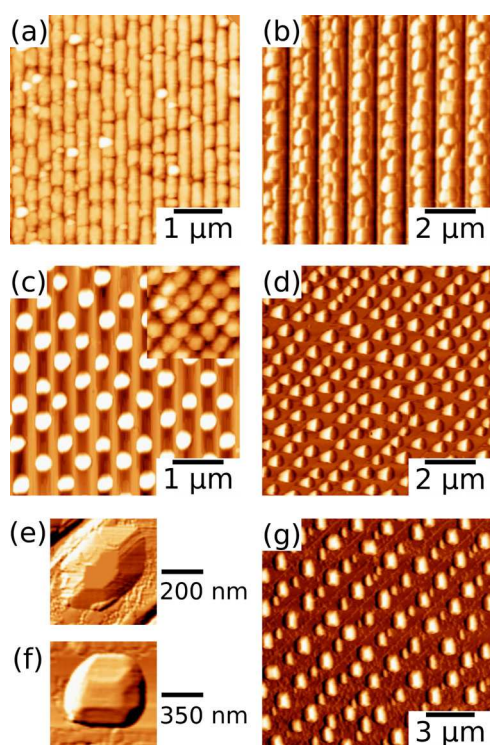


FIG. 3. AFM images after heterogeneous dewetting (EBL patterns) of 11 nm thick c-Si at 750°C : (a) first step is a periodic breaking of the film ($t = 10$ min); (b) second step is the periodic alignment of NCs along the dewetted fronts along [110] ($t = 30$ min); (c) bi-dimensional periodic ordering of NCs induced when matching the NCs size and the pre-patterns 500 nm period ($t = 120$ min). The inset shows the same behaviour for a smaller period of the patterns (~ 200 nm); (d) ordering of NCs along [100] lines ($t = 30$ min); (e) zoom of these NCs; (f) zoom of the NCs shape after longer annealing ($t = 120$ min); (g) bi-modal NCs size and periodicity after $t = 120$ min annealing.

con with well faceted equilibrium shape: $\{111\}$, $\{113\}$ facets on the sides, and $\{100\}$ on the top (Figs. 3(f) and 3(g)).

More complex configurations are observed when the volume of matter collected over the width of the mesa between two periodic cracks of the film is larger than the volume of a whole number of NCs. For instance, when this volume is larger than the volume of one NC but smaller than the volume of two NCs, they create a bi-modal periodic array (Fig. 3(g)). As a consequence, dewetting of pre-patterned films enables the self-assembly of NCs to be directed along the initial patterns while a Rayleigh-like instability controllably creates the perpendicular periodicity. This way, bi-dimensional periodic arrays of NCs are achieved when matching the size of the NCs with the periodicity of the patterns.

The use of ultra-high resolution FIB direct nanowriting combined with dewetting produces precise alignments of ultra-small NCs with size and position tunable at will. In the examples presented on Fig. 4, thin films have been prepatterned by FIB to create lines and concentric squares and circles extending over $100 \mu\text{m}$ (pitch ~ 100 nm). They controllably create ad hoc features of well ordered NCs with a mean diameter ~ 25 nm. On these images, the thin a-Ge film was dewetted at 750°C for 30 min.

The designing process developed here can be used to create free patterns of NCs with monodisperse size and ad hoc spatial placement. The layout is produced by the association of dewetting from patterns edge and Rayleigh-like instability. The use of ultra-high resolution LMIS-FIB enables to produce monocrystalline NCs with size, periodicity, and placement tunable as well. It provides routes for the design of specific arrangement of nanostructures for generic applications in nanoelectronics (such as nanocrystal memories and single electron transistor).

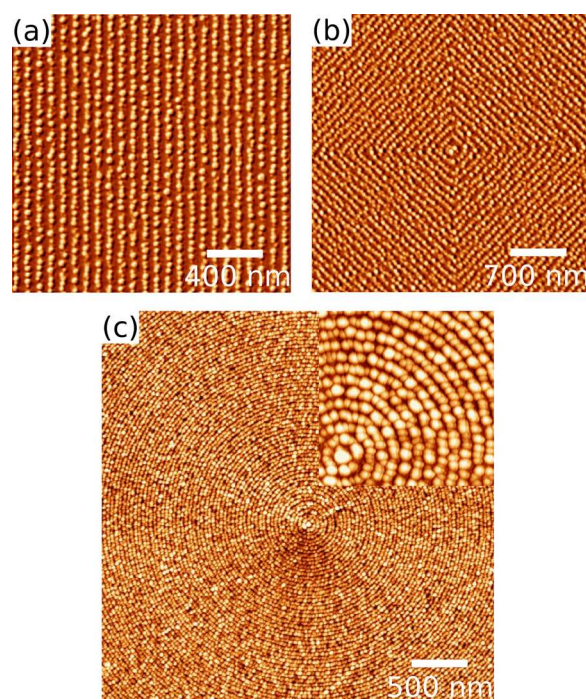


FIG. 4. AFM images of self-organized ultra-small nearly monodisperse Ge NCs (25 nm large) into 2D periodic arrays of lines, squares, and circles using heterogeneous dewetting of FIB patterned 5 nm thick a-Ge ($t = 30$ min; $T = 750^\circ\text{C}$).

- ¹S. Tiwari, F. Rana, H. Hanafi, A. Hartstein, E. F. Crabbé, and K. Chan, *Appl. Phys. Lett.* **68**, 1377 (1996).
- ²Y. Shi, K. Saito, H. Ishikuro, and T. Hiramoto, *J. Appl. Phys.* **84**, 2358 (1998).
- ³E. Kapetanakis, P. Normand, D. Tsoukalas, K. Beltsios, J. Stoemenos, S. Zhang, and J. van den Berg, *Appl. Phys. Lett.* **77**, 3450 (2000).
- ⁴S. Huang and S. Oda, *Appl. Phys. Lett.* **87**, 173107 (2005).
- ⁵L. C. Wu, K. J. Chen, J. M. Wang, X. F. Huang, Z. T. Song, and W. L. Liu, *Appl. Phys. Lett.* **89**, 112118 (2006).
- ⁶Z. Liu, *IEEE Trans. Electron Devices* **49**, 1606 (2002).
- ⁷V. Srcek, M. Kondo, K. Kalia, and D. Mariotti, *Chem. Phys. Lett.* **478**, 224 (2009).
- ⁸H. Vach, *Nano Lett.* **11**, 5477 (2011).
- ⁹F. Gallego-Gomez, M. Ibisate, D. Golmayo, F. J. Palomares, M. Herrera, J. Hernandez, S. I. Molina, A. Blanco, and C. Lopez, *Adv. Mater.* **23**, 5219 (2011).
- ¹⁰D. Song, E. C. Cho, Y. H. Cho, G. Conibeer, Y. Huang, S. Huang, and M. A. Green, *Thin Solid Films* **516**, 3824 (2009).
- ¹¹M. J. Beck and S. T. Pantelides, *Phys. Rev. B* **79**, 033203 (2009).
- ¹²J. H. Jeon, J. Y. Choi, W. W. Park, S. W. Moon, K. W. Park, S. H. Lim, and S. H. Han, *Nanotechnology* **22**, 285605 (2011).
- ¹³B. S. Sahu, F. Gloux, A. Slaoui, M. Carrada, D. Muller, J. Groenen, C. Bonafos, and S. Lhostis, *Nanoscale Res. Lett.* **6**, 177 (2011).
- ¹⁴J. K. Kim, K. M. Cha, J. H. Kang, Y. Kim, J. Y. Yi, T. H. Chung, and H. J. Bark, *Appl. Phys. Lett.* **85**, 1595 (2004).
- ¹⁵R. Peibst, T. Durkop, E. Bugie, A. Fissel, I. Costina, and K. R. Hofmann, *Phys. Rev. B* **79**, 195316 (2009).
- ¹⁶H. Coffin, C. Bonafos, S. Schamm, N. Cherkashin, G. B. Assayag, A. Claverie, M. Respaud, P. Dimitrakis, and P. Normand, *J. Appl. Phys.* **99**, 044302 (2006).
- ¹⁷J. Wang, X. F. Wang, Q. Li, A. Hryciw, and A. Meldrum, *Philos. Mag.* **87**, 11 (2007).
- ¹⁸I. Berbezier and A. Ronda, *Surf. Sci. Rep.* **64**, 47 (2009).
- ¹⁹R. Nuryadi, Y. Ishikawa, and M. Tabe, *Appl. Surf. Sci.* **159**, 121 (2000).
- ²⁰P. P. Zhang, E. P. Nordberg, B. N. Park, G. K. Celler, I. Knezevic, P. G. Evans, M. A. Eriksson, and M. G. Lagally, *New J. Phys.* **8**, 200 (2006).
- ²¹G. Capellini, G. Ciasca, M. De Seta, A. Notargiacomo, F. Evangelisti, and M. Nardone, *J. Appl. Phys.* **105**, 093525 (2009).
- ²²P. Sutter, W. Ernst, Y. S. Choi, and E. Sutter, *Appl. Phys. Lett.* **88**, 141924 (2006).
- ²³W. W. Mullins, *J. Appl. Phys.* **30**, 77 (1959).
- ²⁴J. P. Ye and C. V. Thompson, *Acta Mater.* **59**, 582 (2011).
- ²⁵J. J. Eggleston, G. B. McFadden, and P. W. Voorhees, *Physica D* **150**, 91 (2001).
- ²⁶Z. Suo and Z. Zhang, *Phys. Rev. B* **58**, 5116 (1998).
- ²⁷D. A. Bonnell, *Acta Mater.* **46**, 2263 (1998).
- ²⁸M. Dufay and O. Pierre-Louis, *Phys. Rev. Lett.* **106**, 105506 (2011).
- ²⁹F. Cheynis, E. Bussmann, F. Leroy, T. Passanante, and P. Muller, *Phys. Rev. B* **84**, 245439 (2011).
- ³⁰D. J. Srolovitz and S. A. Safran, *J. Appl. Phys.* **60**, 255 (1986).
- ³¹E. Dornel, J.-C. Barbé, F. de Crécy, G. Lacolle, and J. Eymery, *Phys. Rev. B* **73**, 115427 (2006).
- ³²E. Sutter, P. Sutter, P. Zahl, P. Rugheimer, and M. G. Lagally, *Surf. Sci.* **532**, 785 (2003).
- ³³D. T. Danielson, D. K. Sparacin, J. Michel, and L. C. Kimerling, *J. Appl. Phys.* **100**, 083507 (2006).
- ³⁴O. Pierre-Louis, A. Chame, and Y. Saito, *Phys. Rev. Lett.* **103**, 195501 (2009).
- ³⁵M. Aouassa, L. Favre, A. Ronda, and I. Berbezier, "The kinetics of dewetting ultra-thin Si layers from silicon dioxide," *New J. Phys.* (to be published).
- ³⁶J. N. Aqua, A. Gouyé, T. Auphan, T. Frisch, A. Ronda, and I. Berbezier, *Appl. Phys. Lett.* **98**, 161909 (2011).
- ³⁷Y. H. Tu and J. Tersoff, *Phys. Rev. Lett.* **98**, 096103 (2007).
- ³⁸I. Berbezier, A. Karmous, A. Ronda, A. Sgarlata, A. Balzarotti, P. Castrucci, M. Scarselli, and M. De Crescenzi, *Appl. Phys. Lett.* **89**, 063122 (2006).
- ³⁹G. Garcia, A. F. Lopeandia, A. Bernardi, M. I. Alonso, A. R. Goni, J. L. Labar, and J. Rodriguez-Viejo, *J. Nanosci. Nanotechnol.* **9**, 3013 (2009).
- ⁴⁰I. Berbezier, A. Karmous, A. Ronda, A. Sgarlata, A. Balzarotti, and M. De Crescenzi, *Mater. Sci. Semicond. Process.* **9**, 812 (2006).
- ⁴¹K. Gacem, A. El Hdiy, M. Troyon, I. Berbezier, P. D. Szkutnik, A. Karmous, and A. Ronda, *J. Appl. Phys.* **102**, 093704 (2007); K. Gacem, A. El Hdiy, M. Troyon, I. Berbezier, and A. Ronda, *Nanotechnology* **21**, 065706 (2010).
- ⁴²M. Scarselli, S. Masala, P. Castrucci, M. De Crescenzi, E. Gatto, M. Venanzi, A. Karmous, P. D. Szkutnik, A. Ronda, and I. Berbezier, *Appl. Phys. Lett.* **91**, 141117 (2007).
- ⁴³C. B. Simmons, M. Thalakulam, B. M. Rosemeyer, B. J. Van Bael, E. K. Sackmann, D. E. Savage, M. G. Lagally, R. Joynt, M. Friesen, S. N. Coppersmith, and M. A. Eriksson, *Nano Lett.* **9**, 3234 (2009).
- ⁴⁴E. S. M. Goh, T. P. Chen, S. F. Huang, Y. C. Liu, and C. Q. Sun, *J. Appl. Phys.* **109**, 064307 (2011).
- ⁴⁵P. Zhang, E. Tevaarwerk, B. N. Park, D. E. Savage, G. K. Celler, I. Knezevic, P. G. Evans, M. A. Eriksson, and M. G. Lagally, *Nature (London)* **439**, 04501 (2006).
- ⁴⁶T. C. Chang, F. Y. Jian, S. C. Chen, and Y. T. Tsai, *Mater. Today* **14**, 608 (2011).
- ⁴⁷J. Ye and C. V. Thompson, *Adv. Mater.* **23**, 1567 (2011).
- ⁴⁸The SOI samples (CEA-Leti, France) were fabricated by the Smart Cut™ process.
- ⁴⁹G. Benassayag and P. Sudraud, *Scanning Microsc.* **2**, 1329 (1988).
- ⁵⁰P. Sudraud, P. Ballongue, J. Vandewalle, and C. Colliex, *Ultramicroscopy* **5**, 236 (1980).
- ⁵¹G. Benassayag, P. Sudraud, and L. W. Swanson, *Surf. Sci.* **181**, 362 (1987).
- ⁵²W. K. Choi, T. H. Liew, H. G. Chew, F. Zheng, C. V. Thompson, Y. Wang, M. H. Hong, X. D. Wang, L. Li, and J. Yun, *Small* **4**, 330 (2008).
- ⁵³A. Karmous, I. Berbezier, A. Ronda, R. Hull, and J. Graham, *Surf. Sci.* **601**, 2769 (2007).